# Precise Orbit Determination on LEO Satellite using Pseudorange and Pseudorange-Rate Measurements

Andrea TANTUCCI[1,*], Andrea WRONA[1], and Antonio PIETRABISSA[1]

***Abstract*— Nowadays, along with the trend of developing highly autonomous satellites, there is a strong motivation to improve real-time Precise Orbit Determination (POD), in particular for Low Earth Orbit (LEO) satellites. The development of Global Navigation Satellite System (GNSS) sensors allows to obtain low-noise measurements and provide a satellite with autonomous continuous tracking onboard. Following the deactivation of Selective Availability, a representative real-time positioning accuracy of 10 m is presently achieved by means of Global Positioning System (GPS) receivers on LEO satellites. The introduction of dynamical filtering methods has opened a new way to improve this accuracy by making use of measurements such as pseudorange or carrier-phase. This paper presents a Kalman filtering approach using pseudorange and pseudorange-rate measurements instead of pseudorange and carrier-phase ones, with advantages in terms of storage and processing requirements. An error of around 0.2 m and 1e-3 m/s for position and velocity is obtained, which is in line if not better w.r.t. other approaches.**

***Index Terms*— Precise Orbit Determination, LEO satellites, Extended Kalman Filter, GNSS Measurements**

## I. INTRODUCTION

The POD problem is one of the most important aspects characterizing satellite mission operations. It consists in the accurate prediction of the satellite ephemeris by estimating the satellite position and velocity based on a sequence of GNSS observations.

GPS receivers are widely used on LEO satellites due to the global coverage offered by the GPS constellation which allows a wide number of observations to be processed at the same time, differently from the Medium Earth Orbit (MEO) and Geosynchronous Earth Orbit (GEO) orbits, in which a reduced number of usable satellites, high values of Geometric Diluition Of Precision (GDOP) and significant GNSS outage periods do not allow a precise estimation of the satellite position and velocity.

A 10 m and 0.1 m/s navigation accuracy for position and velocity, respectively, is generally considered adequate for Attitude and Orbit Control Systems (AOCS). Following the deactivation of Selective Availability, this accuracy can readily be provided by the kinematic navigation solution using a single-frequency GPS receiver. However, much higher accuracy is required in many onboard navigation tasks, such as SAR interferometry or atmospheric sounding. These cases call for a sub-decimeter position accuracy and a sub-mm/s velocity knowledge. In the past, this accuracy could be obtained in a ground-based reduced dynamic orbit determination using dual-frequency carrier phase measurements along with precise GPS ephemeris products and auxiliary environmental information. To improve the accuracy of the onboard navigation solutions, Kalman filtering techniques have been broadly used, finding applications in both attitude [1], [2] and orbit propagation control schemes [3], [4]. In [5] the author compares the use of the Unscented Kalman Filter (UKF) approach with the Extended Kalman Filter (EKF) one with different types of measurements: GPS navigation solutions (position and velocity of the satellite obtained by least squares of the GNSS measurements) and pseudorange measurements. It is shown that the latter method improves the accuracy: in particular, a maximum accuracy of about $12$ m for the position and $0.0159$ m/s for the velocity at convergence is obtained. [6] proposes a novel approach using the Schmidt Consider Kalman Filter (CKF). This approach is able to obtain a high level of accuracy also in the presence of uncertainties in the model parameters by partitioning the filter state into actual estimation variables and uncertain parameters variables. The latter ones are mantained constant during the propagation and are not corrected by the measurements.

In this paper, an EKF estimation algorithm has been considered. The measurements which have been considered are the pseudorange and the pseudorange-rate. On the one hand, it will be shown that the use of multiple GNSS measurements increases the accuracy by a huge margin w.r.t. using only one of them as in [5], which uses the pseudorange measurement only. On the other hand, [7] and [8] use the carrier-phase instead of the pseudorange-rate since it allows to mitigate some of the measurement errors. However, the use of carrier-phase measures introduces new state variables to be estimated in the form of ambiguity biases, whose number varies at every observation instant since it corresponds to the number of tracked satellites. The dynamic augmentation of the filter state increases the storage and computational load of the satellite hardware, which might be significant in small LEO satellites. The use of the pseudorange-rate instead (which is the Doppler signal expressed in m/s), allows to obtain an accuracy below the 1 m threshold for the position and below the $0.001$ m/s threshold for the velocity, without increasing the filter state dimension as in the previous approaches, therefore reducing the storage and computational load for the onboard processor. This is also an improvement w.r.t. [4], where an accuracy of $10$ meters ($1\ \sigma$) for the position and of $0.01$ m/s ($1\ \sigma$) threshold for the velocity have been obtained by using, as measurements,

[1] Dept. of Computer, Control, and Management Engineering "Antonio Ruberti" – (DIAG), University of Rome "La Sapienza", Rome, Italy
[*] Corresponding author
Email addresses: {tantucci, wrona, pietrabissa}@diag.uniroma1.it

the pseudorange and the Doppler.

We note that, since the focus of this paper is to validate the use of the GNSS measurements, no uncertainties in the model have been considered for the sake of simplicity. Nevertheless, in presence of uncertain parameters a robust filter might be used, as for example the CKF (which reduces to an EKF if no model uncertainties are considered).

The paper is organized as follows: the first section describes the mathematical model of the satellite, also used for the simulations; the second section describes the Extended Kalman Filter theory and the algorithm filter implementation; the third section describes the Matlab simulation environment and defines the GNSS measurement equations; the fourth section presents the simulation results; the last section draws the conclusions.

## II. Mathematical Model of the Satellite Motion

The equation of motion of a LEO satellite can be written in the form of a second-order differential equation in an Earth Centered Inertial (ECI) reference frame:

$$\ddot{\mathbf{r}} = \ddot{\mathbf{r}}_{GRAV} + \ddot{\mathbf{r}}_{DRAG} + \ddot{\mathbf{r}}_{SRP}, \tag{1}$$

where $\ddot{\mathbf{r}}$ is the satellite acceleration vector, computed as the sum of the vectors of the accelerations due to the gravity, $\ddot{\mathbf{r}}_{GRAV}$, the atmospheric drag, $\ddot{\mathbf{r}}_{DRAG}$, and the Solar Radiation Pressure (SRP), $\ddot{\mathbf{r}}_{SRP}$.

In turn, $\ddot{\mathbf{r}}_{GRAV}$ is the sum of three contributions:

$$\ddot{\mathbf{r}}_{GRAV} = \ddot{\mathbf{r}}_E + \ddot{\mathbf{r}}_S + \ddot{\mathbf{r}}_M, \tag{2}$$

where $\ddot{\mathbf{r}}_S$ and $\ddot{\mathbf{r}}_M$ are third body perturbations due to the Sun and the Moon, respectively, and $\ddot{\mathbf{r}}_E = -(GM/r^3)\mathbf{r} + \mathbf{g}_E$ is the gravity acceleration of the Earth, where the first term accounts for the effect of the Earth's central body, with $\mathbf{r}$ being the satellite position vector and $GM = 3.986\text{e}14$ $\text{m}^3/\text{s}^2$ being the product between the universal gravitational constant and the Earth's mass, whereas $\mathbf{g}_E$ is the contribution due to the flattening and non-homogeneous mass distribution.

For the gravity modeling, the Earth Gravitational Model (EGM) 2008 [9] has been used, that uses spherical harmonics and associated Legendre functions to characterize the gravity potential. In the considered model, the order $n$ and degree $m$ of the harmonics have been set both to 120: this value has been selected because, for LEO, is high enough to have precise estimation of the gravity acceleration. We note that the accuracy on gravity acceleration obtained with degree and order 120 is significantly higher than the absolute value and accuracy of other perturbation models (especially the drag model because of the uncertainties on the atmosphere density). The general expression for the Third Body contributions, i.e., $\ddot{\mathbf{r}}_S$ and $\ddot{\mathbf{r}}_M$, is given by

$$\ddot{\mathbf{r}}_{TB} = GM_{TB}\Big(\frac{\mathbf{d}-\mathbf{r}}{\|\mathbf{d}-\mathbf{r}\|^3} - \frac{\mathbf{d}}{\|\mathbf{d}\|^3}\Big), \tag{3}$$

where $GM_{TB}$ is the product between the universal gravitational constant and the mass of the third body $M_{TB} \in \{M_s, M_m\}$, $\mathbf{r}$ and $\mathbf{d}$ are the position vectors of the satellite and the third body (Sun and Moon) respectively, expressed in the Earth-centered inertial (ECI) coordinate frames.

The atmospheric drag acceleration is modeled as

$$\ddot{\mathbf{r}}_{DRAG} = -\frac{1}{2}\rho C_d \frac{A}{m}\|\mathbf{V}_r\|^2 \hat{\mathbf{V}}_r, \tag{4}$$

where $C_d$ is the drag coefficient, $\rho$ is the atmospheric density, $A$ is the satellite equivalent drag surface, $m$ is the satellite mass, $\|\mathbf{V}_r\|$ and $\hat{\mathbf{V}}_r$ are the norm and unit vector of the satellite velocity relative to Earth atmosphere $\mathbf{V}_r$, expressed in the ECI reference frame (under the assumption that the atmosphere rotates with the Earth). The computation of the drag acceleration requires the knowledge of atmospheric density profiles, which are subjected to short-term and long-term variations. Since complicated models for atmospheric density cannot be used on-board, due to the limited computational load, the Modified Harris-Priester model [10] has been chosen as an alternative.

For the solar radiation pressure contribution, the following model has been considered [10]:

$$\ddot{\mathbf{r}}_{SRP} = -P_{Ref} C_{sp} \frac{A}{m} \frac{\hat{\mathbf{r}}_{SUN}}{\|r_{SUN}\|^2} d_{Ref}^2, \tag{5}$$

where $P_{Ref}$ is the reference solar radiation pressure at one Astronomical Unit ($d_{Ref}$) from the Sun, $C_{sp}$ is the solar radiation coefficient, $A$ is the satellite surface, $m$ is the satellite mass, $\|\mathbf{r}_{SUN}\|$ and $\hat{\mathbf{r}}_{SUN}$ are the module and the unit vector of the satellite-to-Sun vector $\mathbf{r}_{SUN}$.

## III. On-Board Navigation Algorithm

### A. Extended Kalman Filter Implementation

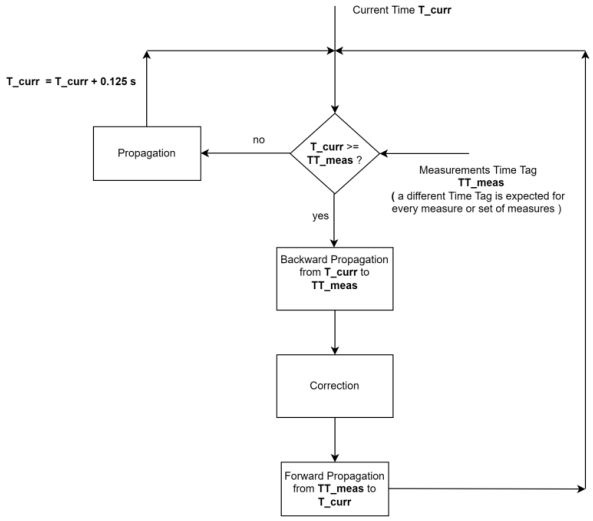


Fig. 1. Extended Kalman Filter Implementation Flow Chart

Necessarily, due to the large non-linearities in the GNSS observation equations and in the dynamical model of the satellite motion, a non-linear filter has to be applied. The EKF is a dynamical filter which is sub-optimal, since it relies

on the linearization applied to the non-linear discrete filter dynamics

$$\mathbf{x}_k = f(\mathbf{x}_{k-1}, \mathbf{u}_k) + \mathbf{w}_k, \tag{6}$$
$$\mathbf{y}_k = h(\mathbf{x}_k) + \mathbf{v}_k, \tag{7}$$

where $f$ and $h$ are the differentiable state transition and observation functions, respectively, $\mathbf{w}_k$ and $\mathbf{v}_k$ are process and measurement noises which are assumed to be zero-mean and gaussian with covariances $Q_k$ and $R_k$ respectively, and $\mathbf{x}_k$, $\mathbf{y}_k$ and $\mathbf{u}_k$ are the state, output and control vectors of the filter.

The EKF algorithm consists of two main steps: prediction and correction.

*1) Prediction Step:* The prediction step relies on the propagation process equations:

$$\hat{\mathbf{x}}_f(k+1) = f(\hat{\mathbf{x}}_f(k), \mathbf{u}(k)), \tag{8}$$
$$P(k+1) = \Phi P(k) \Phi^T + Q, \tag{9}$$

where $\hat{\mathbf{x}}_f$ is the estimated filter state, $P$ is the *state-error covariance matrix*, $\Phi$ is the state transition matrix and $Q$ is the state noise covariance matrix. In practice, both $P$ and $Q$ are usually considered as diagonal or block diagonal matrices.

*2) Correction Step:* The correction step is performed when a set of measures with an associated Time Tag (time at which the measurements have been taken) are sent to the filter by the receiver and consists of the following equations:

$$\mathbf{z} = \mathbf{y} - \mathbf{h}(\hat{\mathbf{x}}_k) \tag{10}$$
$$K = PH^T(R + HPH^T)^{-1} \tag{11}$$
$$\hat{\mathbf{x}}_k^+ = \hat{\mathbf{x}}_k^- + K\mathbf{z} \tag{12}$$
$$P^+ = (I - KH)P^- \tag{13}$$

where $\mathbf{z}$ is the measurement residual, $\mathbf{y}$ is the actual measurement vector, $H = \dfrac{\partial h(\hat{\mathbf{x}}_k)}{\partial \hat{\mathbf{x}}_{k-1}}$ is the measurement jacobian w.r.t. the state, $R$ is the measurement error covariance matrix, $K$ is the Kalman gain, $\hat{\mathbf{x}}_k^-$ and $\hat{\mathbf{x}}_k^+$ are the states before and after the correction, respectively. The algorithm implementation logic is shown in Figure 1.

### B. Filter State and State Propagation

In the orbit navigation scenario, there are a lot of parameters which need to be taken into account for a good estimation of the satellite position and velocity. Since GNSS measurement equations are considered in the navigation algorithm, the time synchronization biases have to be considered. A standard solution consists in including both the GPS clock bias $\Delta t_R$ and clock drift $\Delta \dot{t}_R$ in the estimation state [7], [11], [4] . The estimation of these two parameters allows a more precise replica of the pseudorange and pseudorange-rate measurements for the filter algorithm. By adding the drag and solar coefficients $\Delta C_d$ and $\Delta C_s p$, respectively, the filter state consists of 10 scalar variables:

$$\mathbf{x} = [\mathbf{r}, \dot{\mathbf{r}}, C_d, C_{sp}, \Delta t_R, \Delta \dot{t}_R]^T. \tag{14}$$

The state of the filter is propagated by numerically integrating the following differential equations:

$$\frac{d\mathbf{r}}{dt} = \dot{\mathbf{r}} \tag{15}$$
$$\frac{d\dot{\mathbf{r}}}{dt} = \ddot{\mathbf{r}}_E + \ddot{\mathbf{r}}_S + \ddot{\mathbf{r}}_M + \ddot{\mathbf{r}}_{DRAG} + \ddot{\mathbf{r}}_{SRP} \tag{16}$$
$$\frac{dC_d}{dt} = 0 \tag{17}$$
$$\frac{dC_{sp}}{dt} = 0 \tag{18}$$
$$\frac{d\Delta t_R}{dt} = \Delta \dot{t}_R \tag{19}$$
$$\frac{d\Delta \dot{t}_R}{dt} = \dot{d} \tag{20}$$

where $\dot{d}$ is the clock frequency aging, which is a commendable parameter and varies from receiver to receiver.

### C. Measurement Equations

The filter measurement equations account for GNSS observed variables which are collected by the GPS receiver, namely, the pseudorange $\rho_i$ and the pseudorange rate $\dot{\rho}_i$. From this paragraph, to differentiate the GNSS quantities from the user ones, the former will be identified by a subscript *SV* (Space-Vehicle). By denoting with $N$ the number of tracked satellites, the observation vector $\mathbf{h}(\hat{\mathbf{x}}_k)$ has the following form

$$\mathbf{h}(\hat{\mathbf{x}}_k) = [\hat{\rho}_1(\hat{\mathbf{x}}_k) \ \dots \ \hat{\rho}_N(\hat{\mathbf{x}}_k) \, \hat{\dot{\rho}}_1(\hat{\mathbf{x}}_k) \ \dots \ \hat{\dot{\rho}}_N(\hat{\mathbf{x}}_k)]^T, \tag{21}$$

where the non-linear observation equations have the following form:

$$\hat{\rho}_i(\hat{\mathbf{x}}_k) = \|\mathbf{r}_{SV} - \hat{\mathbf{r}}\| + c\hat{\Delta} t_R \tag{22}$$
$$\hat{\dot{\rho}}_i(\hat{\mathbf{x}}_k) = \hat{\mathbf{e}}(\dot{\mathbf{r}}_{SV} - \hat{\dot{\mathbf{r}}}) + c\hat{\Delta}\dot{t}_R \tag{23}$$

where $\mathbf{r}_{SV}$ and $\hat{\mathbf{r}}$ are the position vectors of the GNSS satellite and the satellite respectively, $\dot{\mathbf{r}}_{SV}$ and $\hat{\dot{\mathbf{r}}}$ are the velocity vectors of the GNSS satellite and the satellite, respectively, $\hat{\mathbf{e}}$ is the estimated unit line-of-sight vector from the user satellite to the GNSS satellite, $\hat{\Delta} t_R$ and $\hat{\Delta}\dot{t}_R$ are the estimated satellite clock bias and clock drift respectively, $c$ is the speed of light.

## IV. Simulation environment

The performance assessment of the filter is performed in a simulated environment. A Matlab environment is used to simulate orbital propagation, visibility analysis and GNSS measurement equations computation. For the GPS simulation, 30 GPS satellites have been considered. The orbital propagation of the satellite is performed starting from the associated Two-Line Elements (TLE) file data. A keplerian propagation has been performed to align the TLE with the simulation initial epoch chosen by the user: in particular only the mean motion and the RAAN have been propagated considering only the J2 effect [12].

A visibility analysis algorithm is implemented: it returns, at every time instant, the GNSS satellites visible from the

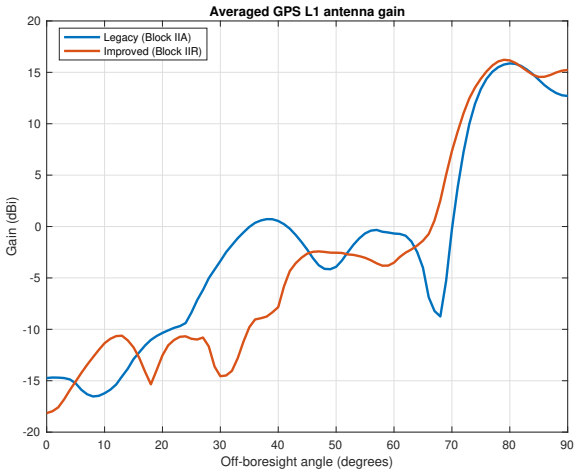


Fig. 2. Antenna Directivity for GPS Block IIA and Block IIR

user satellite, i.e. the ones sending the information needed for the estimation algorithm. In order for a signal to be sent from the GPS satellite and received from the user, two conditions must be satisfied:

1) The GNSS-to-user satellite position vector must be inside both the transmitter and receiver field of view of the antennas, i.e., in their visibility cones;
2) The Carrier to Noise ratio ($C/N_0$) must be over a certain threshold

In particular, the $C/N_0$ is computed in dBHz using the following equation

$$C/N_0 = P_{TX} + G_{TX} - L_{TX} + G_{RX} - L_{RX} - L_{FSL} - N_0, \quad (24)$$

where: $P_{TX}$ is the transmission power of the GPS satellites expressed in dBW; $G_{TX}$ and $G_{RX}$ are the satellite and receiver antenna gains, respectively, measured in dBi (gain w.r.t. an isotropic antenna); $L_{TX}$ and $L_{RX}$ are the transmission and reception losses, respectively, measured in dB; $N_0$ is the Thermal Noise Density, expressed in Kelvin and computed as $N_0 = K_B + T_{sys}$, where $K_B$ is the Boltzmann's constant and $T_{sys}$ is the system noise temperature; $L_{FSL}$ accounts for the Free-Space Losses, and is computed in dB as

$$L_{FSL} = 20\log_{10}(4\pi d/\lambda), \quad (25)$$

with $d$ being the distance from GPS satellite to the user satellite and $\lambda$ being the wavelength of the GPS L1-band (1.58 GHz).

In Figure 2 the GPS antenna gain patterns are shown, i.e. the value of the antenna gain at different elevation values. Since the pattern are symmetric only half of the patterns have been showed. GPS has two patterns: one is called Legacy and is related to a particular block of satellites (IIA) while the other one is called Improved and is related to another block of satellites (IIR) [13]. In the implementation it has been assumed that the maximum gain is at 90 degrees.

For the GNSS measurement computation, the standard formulation [14], [15] has been used for pseudorange and pseudorange rate

$$\rho = \|\mathbf{r}_{SV}(t_{TX}) - \mathbf{r}(t_{Rx})\| + c\Delta t_R + c\Delta t_{SV} + \Delta I + \Delta MP + \epsilon_\rho, \quad (26)$$

$$\dot{\rho} = \mathbf{e}\cdot(\dot{\mathbf{r}}_{SV}(t_{Tx}) - \dot{\mathbf{r}}(t_{Rx})) + c\Delta\dot{t}_R + \epsilon_{\dot{\rho}}, \quad (27)$$

where $\Delta t_{SV}$ is the GPS clock bias, $\Delta I$ is the ionospheric error, $\Delta MP$ is the Multipath error, $t_{TX}$ and $t_{Rx}$ are the transmission and reception epoch, respectively, $c$ is the speed of light. The contributions of these errors have been modeled as gaussian random noises. The clock bias $\Delta t_R$ and clock drift $\Delta\dot{t}_R$ are modeled as a two-state stochastic dynamic model [16], [17]. $\epsilon_\rho$ and $\epsilon_{\dot{\rho}}$ are the receiver measurement errors which represent the errors of the recevier Lock Loops, i.e., the Delay Lock Loop (DLL) for the code pseudorange and Frequency Lock Loop (FLL) for the pseudorange rate. They are modeled as white gaussian noises with standard deviations computed in the following way [18]:

$$\sigma_{DLL} = \left[\frac{B_n}{2C/N_0}\left(\frac{1}{B_{fe}T_c} + \frac{B_{fe}T_c}{\pi - 1}\left(D - \frac{1}{B_{fe}T_c}\right)^2\right)\left(1 + \frac{2}{T(C/N_0)(2-D)}\right)\right]^{\frac{1}{2}} \text{ chips}, \quad (28)$$

$$\sigma_{FLL} = \frac{\lambda}{2\pi T}\sqrt{\frac{4FB_n}{C/N_0}\left[1 + \frac{1}{TC/N_0}\right]} \text{ m/s}, \quad (29)$$

where $B_n$ is the closed loop bandwidth of the loops, $C/N_0$ computed in Hz as $C/N_0 = 10\exp\left(\frac{(C/N_0)_{\text{dB}}}{10}\right)$, $B_{fe}$ is the front-end bandwidth of the receiver, $T_c$ is the chip period, $T$ is the integration time of the correlation process, $D$ is the correlator spacing, $\lambda$ is the wavelength of the receiver frequency, $F$ is 1 for large $C/N_0$ values and 2 for $C/N_0$ values close to the threshold value. Note that the DLL standard deviation is expressed in chips: to convert it in meters, it has to be multiplied by the chip length which is equal to 293.05 m/chip for C/A code and to 29.305 m/chip for P(Y) code.

## V. Simulation Results

The achieved filter performances are presented in terms of position and velocity estimation accuracy w.r.t. the simulated trajectories. The initial conditions have been set starting from the simulated satellite initial conditions, perturbed using gaussian random errors with standard deviations in accordance to the ones collected in Table I. The other states have been initialized to zero. The frequency of GPS measurements is 1 second. The filter propagation time-step $\Delta T$ has been set to 0.125 seconds in order to reduce the delay between the detection of the measurement signals and the filter correction implementation.

TABLE I

TABLES OF FILTER PARAMETERS

| State Initial Covariance $P_0$ | Process Noise Covariance $Q_0$ | Measurement Noise Covariance $R_0$ |
|---|---|---|
| $\sigma_{\mathbf{r}} = 10_{\text{m}}$ | $\sigma_{\mathbf{r}} = [1 \cdot 10^{-6}\, 1 \cdot 10^{-6}\, 5 \cdot 10^{-6}]_{\text{m}}$ | $\sigma_{UERE} = (5.2 + \sigma_{DLL})_{\text{m}}$ |
| $\sigma_{\dot{\mathbf{r}}} = 0.5_{\text{m/s}}$ | $\sigma_{\dot{\mathbf{r}}} = [1 \cdot 10^{-7}\, 1 \cdot 10^{-7}\, 5 \cdot 10^{-7}]_{\text{m/s}}$ | $\sigma_{UERRE} = (0.33 + \sigma_{FLL})_{\text{m/s}}$ |
| $\sigma_{\Delta Cd} = 30^{1/2}$ | $\sigma_{\Delta Cd} = 0.005 \cdot 10^{-3}$ | |
| $\sigma_{\Delta Cs} = 30^{1/2}$ | $\sigma_{\Delta Cs} = 0.005 \cdot 10^{-3}$ | |
| $\sigma_{\Delta t_R} = 100_{\text{m}}$ | $Q_{\Delta t_R, \Delta \dot{t}_R} = \begin{bmatrix} 1.2565 \cdot 10_{\text{m}}^{-5} & 5 \cdot 10^{-8} \\ 5 \cdot 10^{-8} & 1.2565 \cdot 10_{\text{m/s}}^{-7} \end{bmatrix}$ | |
| $\sigma_{\Delta \dot{t}_R} = 100_{\text{m/s}}$ | | |

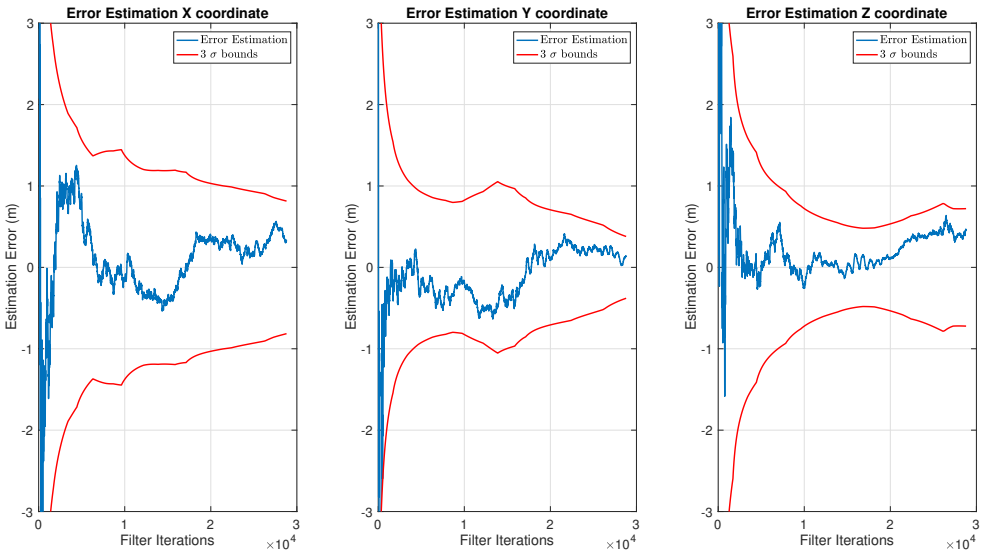


Fig. 3. Position Error with pseudorange measurements and 3-sigma bounds.

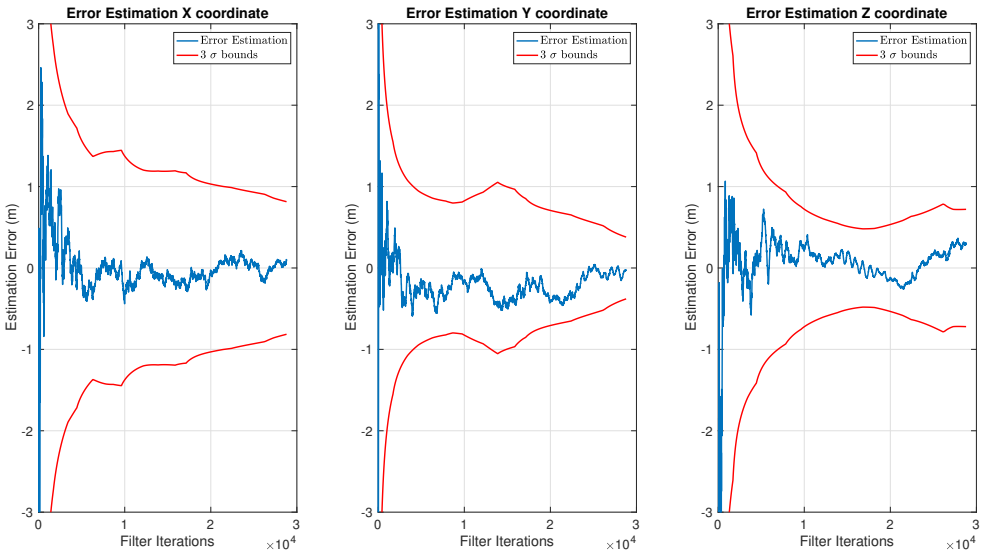


Fig. 4. Position Error with both pseudorange and pseudorange-rate measurements and 3-sigma bounds

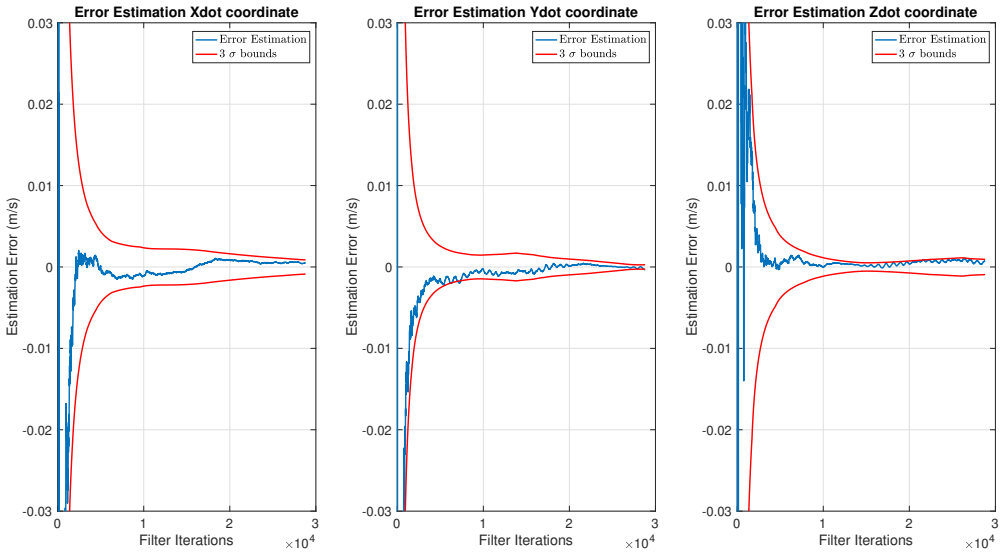


Fig. 5. Velocity Error with only pseudorange measurements and 3-sigma bounds

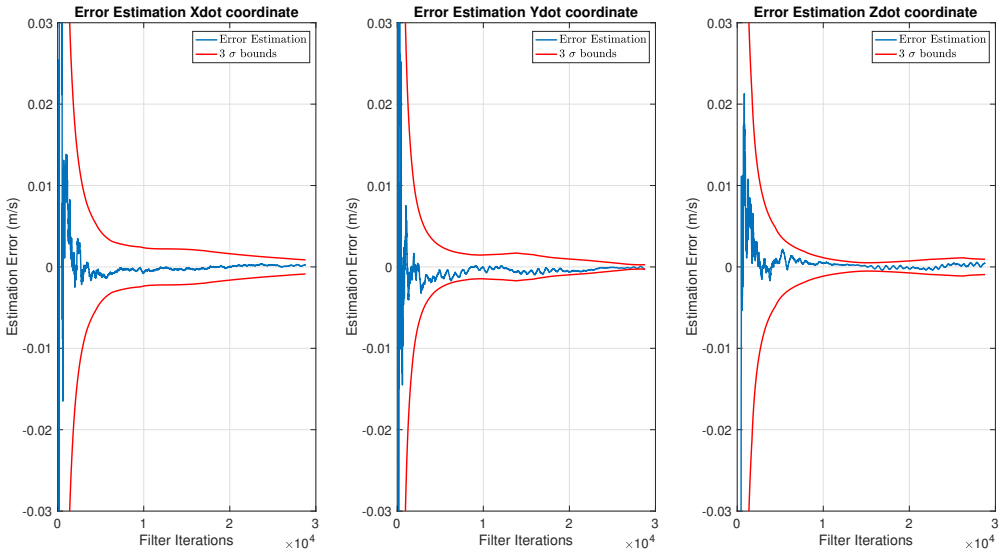


Fig. 6. Velocity Error with both pseudorange and pseudorange-rate measurements and 3-sigma bounds

The accuracy of the estimation is further analyzed by introducing 3-$\sigma$ bounds which have to be satisfied during the whole simulation. The introduction of these bounds allows to understand what is the estimation error with a confidence value of 99.7.

The process noise covariance of the clock bias and clock drift has been defined as a full matrix denoted by $Q_{\Delta t_R, \Delta \dot{t}_R}$, with cross-covariance different from zero according to [16], [17], [19].

To validate the introduction of the pseudorange-rate measurements, the algorithm is compared with the approach used in [5], where only pseudorange measurements are used for POD. The same filter parameters (the ones in Table I) are used for both the algorithms. The simulation time is 1 hour. Figures 3 and 4 show the position errors with the corresponding 3-$\sigma$ bounds which are obtained by using only pseudorange and both pseudorange and pseudorange-rate, respectively. It can be seen how the convergence of the algorithm is faster in the second case: there is a huge improvement for the **x** axis, whose error oscillations are minimal after 15000 iterations (about 31 minutes) while in the first case after 1 hour the error still has some peaks. The **y** component is quite similar while for the **z** component the second algorithm has a better transient in particular in the early stages of the filter.

Figures 5 and 6 show the velocity estimation errors in the two cases. The difference in the convergence time is improved by the proposed algorithm: the error oscillations tend to stabilize after 5000 iterations (about 10 minutes) when both measurements are used, while in the case of a single measurement after 15000 iterations (about 31 minutes). In both cases the error stabilizes around a very small value near zero. It is important to notice that in the first case there are some intervals in which the error curve is out of the covariance bounds, while in the second case the error remains inside the $3\,\sigma$ bounds.

## VI. Conclusions

This paper presented an Extended Kalman Filter algorithm for Precise Orbit Determination. The algorithm uses pseudorange and pseudorange-rate as measurements to improve the accuracy in position and velocity estimation error without affecting the storage and computational complexity of the filter, as occurs, for instance, in the solutions based on pseudorange and carrier-phase measures. It has been shown how the error dynamics satisfies the covariance bounds and how the accuracy is below 1 meter for the position estimation error and one order of magnitude below the acceptable level (0.1 m/s) for the velocity estimation error. This is due to the introduction of the pseudorange-rate measure along with the pseudorange one, which guarantees a direct measure of the velocity and has a direct impact on the H-matrix of the filter: simulation runs show that, by adding the pseudorange rate measure, the algorithm guarantees faster convergence in particular for the velocity estimation which is 3 times faster.

The approach presented in this work is a simplification of the real case scenario in the fact that some quantities in the measurements equations (multipath, ionospheric delay,..) have been modeled as gaussian noises. Moreover it is not able to cope with the presence of uncertain parameters in the model as well as the CKF. A possible future scenario may consist into the implementation of actual models for these errors analyzing if the pseudorange and pseudorange rate-based EKF is able to maintain an acceptable level of accuracy and under which conditions.

## References


[1] D. Menegatti, A. Giuseppi, and A. Pietrabissa, "Model predictive control for collision-free spacecraft formation with artificial potential functions," in *2022 30th Mediterranean Conference on Control and Automation (MED)*, pp. 564–570, IEEE, 2022.

[2] A. Giuseppi, A. Pietrabissa, S. Cilione, and L. Galvagni, "Feedback linearization-based satellite attitude control with a life-support device without communications," *Control Engineering Practice*, vol. 90, pp. 221–230, 2019.

[3] Y. Feng, "An alternative orbit integration algorithm for gps-based precise leo autonomous navigation," *GPS Solutions*, vol. 5, pp. 1–11, 2001.

[4] R. C. Hart, K. R. Hartman, A. C. Long, T. Lee, and D. H. Oza, "Global positioning system (gps) enhanced orbit determination experiment (geode) on the small satellite technology initiative (ssti) lewis spacecraft," *Proceedings of the ION-GPS-1996, Kansas City, MO, USA*, pp. 17–20, 1996.

[5] E.-J. Choi, J.-C. Yoon, B.-S. Lee, S.-Y. Park, and K.-H. Choi, "Onboard orbit determination using gps observations based on the unscented kalman filter," *Advances in Space Research*, vol. 46, no. 11, pp. 1440–1450, 2010.

[6] R. Zanetti and C. D'Souza, "Recursive implementations of the schmidt-kalman 'consider'filter," *The Journal of the Astronautical Sciences*, vol. 60, no. 3-4, pp. 672–685, 2013.

[7] M. O. Karslioglu, E. Erdogan, and O. Pamuk, "Gps-based real-time orbit determination of low earth orbit satellites using robust unscented kalman filter," *Journal of Aerospace Engineering*, vol. 30, no. 6, p. 04017063, 2017.

[8] S. Kavitha, P. Mula, M. Kamat, S. Nirmala, and J. G. Manathara, "Extended kalman filter-based precise orbit estimation of leo satellites using gps range measurements," *IFAC-PapersOnLine*, vol. 55, no. 1, pp. 235–240, 2022.

[9] N. K. Pavlis, S. A. Holmes, S. C. Kenyon, and J. K. Factor, "The development and evaluation of the earth gravitational model 2008 (egm2008)," *Journal of geophysical research: solid earth*, vol. 117, no. B4, 2012.

[10] O. M. E. Gill and O. Montenbruck, *Satellite orbits*. Springer, 2013.

[11] O. Montenbruck and P. Ramos-Bosch, "Precision real-time navigation of leo satellites using global positioning system measurements," *GPS solutions*, vol. 12, pp. 187–198, 2008.

[12] W. J. Larson, J. R. Wertz, *et al.*, *Space mission analysis and design*, vol. 3. Springer, 1992.

[13] W. Marquis, "The gps block iir/iir-m antenna panel pattern rev 3," *LMCO 2013*, 2013.

[14] P. J. Teunissen and O. Montenbruck, *Springer handbook of global navigation satellite systems*, vol. 10. Springer, 2017.

[15] G. Seeber, *Satellite geodesy*. Walter de gruyter, 2003.

[16] C. Zucca and P. Tavella, "The clock model and its relationship with the allan and related variances," *IEEE transactions on ultrasonics, ferroelectrics, and frequency control*, vol. 52, no. 2, pp. 289–296, 2005.

[17] L. Galleani, L. Sacerdote, P. Tavella, and C. Zucca, "A mathematical model for the atomic clock error," *Metrologia*, vol. 40, no. 3, p. S257, 2003.

[18] E. D. Kaplan and C. Hegarty, *Understanding GPS/GNSS: principles and applications*. Artech house, 2017.

[19] L. Galleani, "A tutorial on the two-state model of the atomic clock noise," *Metrologia*, vol. 45, no. 6, p. S175, 2008.